Effects of neutron number and nuclear deformation on complete fusion of ^{60,64}Ni+^{154}Sm near the Coulomb barrier

S. Mitsuoka, H. Ikezoe, K. Nishio, K. Satou, and J. Lu
Advanced Science Research Center, Japan Atomic Energy Research Institute, Tokai Ibaraki, 319-1195, Japan
(Received 8 October 2001; published 1 May 2002)

In order to study the effects of heavy projectile neutron number on complete fusion with a well-deformed target, we have measured the excitation functions of the evaporation residue cross sections for xn, pxn, and αxn channels ($x=2$–6) by using the JAERI recoil mass separator in the reactions of ^{60}Ni+^{154}Sm and ^{64}Ni+^{154}Sm at energies around the Coulomb barrier. In the ^{64}Ni-induced reaction, the evaporation residue cross section was larger by about two orders of magnitude than that in the ^{60}Ni-induced reaction. This is mainly due to the exit channel effect of the small neutron separation energy in the more neutron-rich compound nucleus. The fusion probability has been obtained from the calculated survival probability, which had agreed with the evaporation residue cross sections measured in the same compound nucleus system of ^{32}S+^{182}W. No obvious difference in the extracted fusion probability between the ^{64}Ni- and ^{60}Ni-induced fusion reactions was observed in the excitation functions. In both reaction systems, the fusion probabilities at the lowest energies, where collisions only at the tip of the deformed ^{154}Sm nucleus are possible, were significantly smaller than the coupled channel calculation by three orders of magnitude. On the other hand, fusion hindrance was negligible at higher energies where side collisions with the deformed ^{154}Sm become possible. This is consistent with our previous conclusion that tip collisions need some extra kinetic energy over the fusion barrier in order to fuse, while side collisions lead to complete fusion without such extra energy.

DOI: 10.1103/PhysRevC.65.054608 PACS number(s): 25.70.Jj, 25.70.Gh, 24.60.Dr, 27.80.+w

I. INTRODUCTION

The synthesis of transactinide (superheavy) elements approaching the predicted double magic nucleus with $N=184$ and $Z=114$ (and/or 126) is an important current topic in nuclear physics. Superheavy elements have been formed via either one neutron ($1n$) evaporation channel in cold fusion reactions [1] or via $4n$ and $5n$ channels in hot fusion reactions [2]. These types of fusion-evaporation reactions have been the most successful methods to produce superheavy elements so far, but unfortunately the production cross sections of the heaviest elements are close to the sensitivity limit of present day experimental techniques. In order to search for a new approach to the superheavy region with measurable cross sections, many experimental and theoretical possibilities have been explored.

One of the most promising solutions is the cold fusion reaction of two closed-shell nuclei [3]. In addition to doubly magic ^{208}Pb- and ^{209}Bi-based cold fusion with the $N=50$ magic projectile of ^{86}Kr, ^{87}Rb, or ^{88}Sr [4], more symmetric projectile-target combinations between $N=82$ magic nuclei of ^{136}Xe, ^{138}Ba, or ^{140}Ce have been proposed [5]. Another possibility is to use intense radioactive beams for producing more neutron-rich superheavy elements. Many authors have suggested that there will be an enhancement of the sub-barrier fusion cross sections for very n-rich projectiles due to their extended neutron density distribution far beyond the range of normal β-stable nuclei.

Among some other possibilities of synthesizing superheavy elements, an appealing speculation has been theoretically proposed; a gentle fusion [6] or a hugging fusion [7] by using well-deformed nuclei as colliding partners. The combinations of rare-earth nuclei, e.g., Nd, Sm, Gd, and Dy with large deformations ($\beta_2\sim0.3$) would yield compound systems around $Z=126$ and $N=184$ [6]. In this type of fusion reaction, the relative orientation of the symmetry axes of the deformed nuclei significantly changes the Coulomb barrier height at the touching point. In different varieties of the touching configuration, hugging fusion takes place when the symmetry axes are orthogonal to each other. This specific configuration has two characteristic features. First, this fusion configuration has the most compact shape. Second, the orthogonal configuration leads to a fusion path far from the axial-symmetric fission path. It is predicted that this compact configuration would lead to high formation probability in the entrance channel.

In order to check this speculation experimentally, we have started to investigate sub-barrier fusion with strongly deformed nuclei of ^{154}Sm ($\beta_2=0.32$), ^{182}W ($\beta_2=0.28$), and ^{150}Nd ($\beta_2=0.36$). To obtain direct evidence that the heavy projectile really fuses with the deformed target, the fusion-evaporation residues emitted along the beam direction were separated by the JAERI recoil mass separator (RMS) [8] and identified on the basis of time- and position-correlated α decays. The angular distributions of fission fragments were also measured around the target to obtain the total fusion cross section. The experimental results have recently been published in Ref. [9] for the reactions of ^{60}Ni+^{154}Sm and ^{32}S+^{182}W, where the same compound nucleus ^{214}Th is formed, and also in Ref. [10] for the reactions of ^{76}Ge+^{150}Nd and ^{28}Si+^{198}Pt, where the compound nucleus ^{226}U is formed. By comparing two reaction systems that make the same compound nucleus, one can discuss the effect of target deformation on the fusion process in the entrance channel, because the survival process against fission in the exit channel is the same. Moreover, in Ref. [11], the effect of nuclear deformation in the $^{76}Ge+^{150}Nd$ reaction has been directly compared with the case of spherical projectile and target combination in the $^{82}Se+^{nat}Ce$ reaction.

In these papers, we showed that the fusion probability depends strongly on the orientation of nuclear deformation. When the projectile collides at the tip of the deformed target (hereafter called tip collision), the distance between the two mass centers at the contact point is the largest. Consequently the Coulomb barrier height becomes minimum, but the shape of the touching configuration is much elongated. In a side-to-side collision (hereafter called side collision), on the other hand, the barrier height becomes maximized but the touching configuration is the most compact. It is of interest to understand which type of collision is more favorable for heavy-element synthesis. In light systems, it is expected that tip collisions have the advantage of lowering the Coulomb barrier height. In fact, in the $^{32}S+^{182}W$ and $^{28}Si+^{198}Pt$ reactions of light projectiles with deformed nuclei, we observed a large fusion enhancement over the prediction of the one-dimensional barrier penetration model at energies below the Bass barrier. This can be well explained by taking into account static deformations as well as couplings to the inelastic excitations of the colliding nuclei. On the contrary, in reactions involving heavy projectile-target combinations, complete fusion was significantly hindered even if the incident energy exceeded the Coulomb barrier. Such fusion hindrance is well known as the extra-push phenomenon, which has been widely observed in reactions between massive nuclei, as the charge product Z_1Z_2 of the projectile and target increases beyond $\sim$1800 or the effective fissility parameter χ_{eff} beyond $\sim$0.73. For the synthesis of heavy and superheavy elements, one of the key issues is how to reduce this large hindrance of the heavy-ion fusion probability in the entrance channel.

A clue to the solution is the fact that, even in the heavy projectile systems of $^{60}Ni+^{154}Sm$ ($Z_1Z_2=1736$, $\chi_{eff}=0.735$) and $^{76}Ge+^{150}Nd$ (1920, 0.749) [9,10], there was little fusion hindrance observed at energies near and above the Bass barrier, where side collisions mainly contribute. This suggests that side collisions may lead the system more easily to complete fusion than tip collisions. It is worth relating this to the distance between the two mass centers at the contact point, as expected in cold fusion, where two shell closures can merge inside the contact point without energy dissipation [3,12]. In general, the contact point of massive colliding partners is located outside the fission saddle point of the compound nucleus because the fission saddle shape rapidly becomes more compact than the fusion touching configuration with increasing mass value. When the incident energy is just enough to overcome the fusion barrier, the system will easily evolve towards the fission valley and reseparate without forming a compound nucleus (referred to as first fission or quasifission). To surmount the fission saddle point in the course of compound nuclear formation, an extra kinetic energy called extra-extra-push energy is needed. In the previous cases of $^{60}Ni+^{154}Sm$ and $^{76}Ge+^{150}Nd$, the distance between the mass centers at a side collision is the shortest and is very close to the position of the saddle point, whereas the maximum distance corresponding to a tip collision is well outside the saddle point. This means that the compound nucleus could be more easily formed in the compact touching configuration through a side collision than in the elongated one through a tip collision.

In the present work, we have investigated this effect in a more detailed way by making two improvements; (i) the statistics of the evaporation residue cross sections were increased by an order of magnitude at $E_{c.m.}=182$ MeV in the $^{60}Ni+^{154}Sm$ system because our previous measurements below this energy gave only an upper limit of a few nanobarns, and (ii) excitation functions were measured by using a ^{64}Ni beam having four more neutrons than ^{60}Ni, especially to see how the *n*-rich projectile acts on the fusion probability. The latter also would be helpful to the intriguing aspect of near future experiments using intense *n*-rich radioactive beams. In the future section, we describe the experimental procedure and results for the $^{64}Ni+^{154}Sm$ reaction. In Sec. III, the possible fusion hindrance and enhancement of the evaporation residue cross sections in the xn, pxn, and αxn channels are discussed on the basis of the calculated survival probability, where the parameters used have been determined in the previous analysis of $^{32}S+^{182}W$ ($Z_1Z_2=1184$, $\chi_{eff}=0.613$) [9]. The entrance channel effects of extra neutron number on complete fusion with a well-deformed target are also discussed by comparing directly the data in the ^{60}Ni and ^{64}Ni projectile systems. In Sec. V, we give a summary and some concluding remarks.

II. EXPERIMENTAL PROCEDURE AND RESULTS

The experiments were carried out at the tandem-booster facility of the Japan Atomic Energy Research Institute (JAERI). Details of the experimental procedure are described in our previous papers [9,10], and only the essential points and the experimental results in the present $^{64}Ni+^{154}Sm$ reaction are presented here.

Beams of ^{64}Ni and ^{60}Ni (4–5 MeV/nucleon) were used to bombard a thin target of ^{154}Sm (oxide, 350 $\mu g/cm^2$, 98.6% enriched), which was prepared by sputtering with 30-keV Ar ions onto 0.7-μm aluminum foils. The target foils were mounted on a rotating wheel 80 mm in diameter and rotated at 100 rpm. Rutherford scattering was monitored at a forward angle of $\theta_L=45°$ by a small-area solid state detector for normalization of the cross section measurements. Evaporation residues (ERs) emitted from the target along the beam direction were separated in-flight by the RMS from the primary beam and the background of other reaction products. The primary beam was stopped by a large-area Faraday cup located behind the first electric dipole without hitting the anode surface so as to reduce a background originating from beam scattering at the anode [8]. The Faraday cup also enabled the beam current to be monitored during the experiment.

For the present measurements of low-yield ERs of subnanobarn cross sections, it is important to use the RMS with a large transmission efficiency and low background. In order to provide a large angular acceptance (20 msr) and an energy acceptance ($\pm$12%) while keeping good beam suppression, the ion-optical parameters of the RMS were set to make the

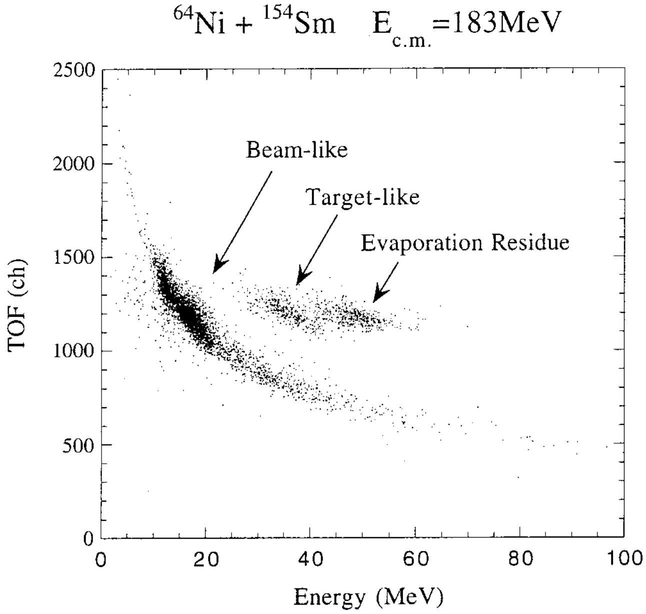

FIG. 1. Two-dimensional matrix between the energy and the TOF of particles incident on the focal plane detectors in the ^{64}Ni $+^{154}$Sm reaction at $E_{\mathrm{c.m.}}=183$ MeV ($E_{beam}=269$ MeV). Events originating from evaporation residues are clearly separated from the backgrounds of beamlike and targetlike particles passing through the RMS.

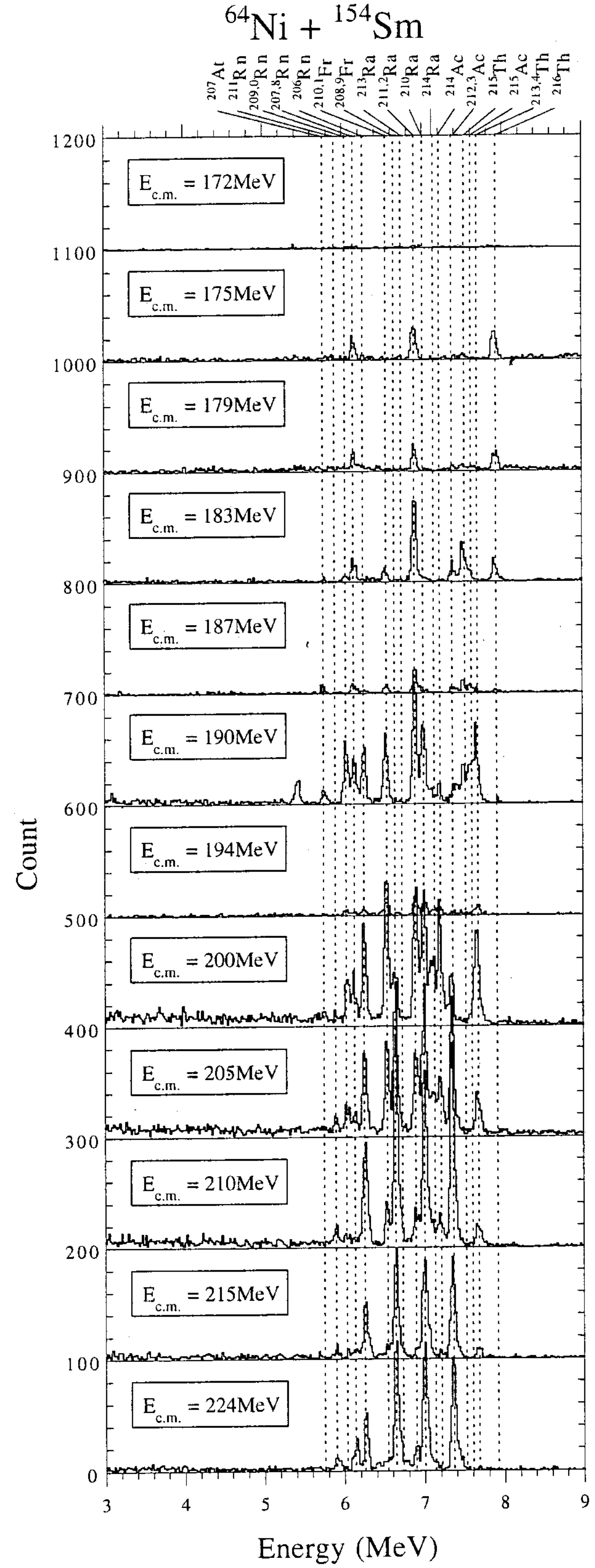

FIG. 2. Measured singles energy spectra of the PSSD in anticoincidence with the TOF signal at all incident energies in the ^{64}Ni $+^{154}$Sm reaction. The dashed lines indicate α-decay energies of known isotopes.

mass dispersion zero at the focal plane [13]. In this setting, some amounts of background could pass through the RMS, when the corresponding nuclei have the same ratios of mass and energy to charge as the ERs of interest. To extract the ERs from such a background, they were passed through two thin-foil timing detectors consisting of microchannel plates separated by a distance of 30 cm, in order to provide a time-of-flight (TOF) signal. Then they were implanted into a double-sided position sensitive silicon detector (PSSD) in order to measure the kinetic energy and two-dimensional positions. Figure 1 shows a typical two-dimensional matrix between the TOF and kinetic energy of the implanted particles in the reaction of ^{64}Ni$+^{154}$Sm at $E_{\mathrm{c.m.}}=183$ MeV ($E_{beam}=269$ MeV). ERs are clearly separated from the background of beamlike and targetlike particles passing through the RMS. The total event rate was about a few counts per second for a typical beam intensity of $10-35$ particle nA.

The implanted ERs, which were produced through xn, pxn, and αxn evaporation channels ($x\sim 2-6$) from the compound nucleus ^{218}Th or ^{214}Th, subsequently α decay and then β decay toward the β-stability line. Because their α-decay branching ratios are nearly 100% and the half-life is of the order of 1 msec, which is longer than the flight time through the RMS and also the dead time of the detection system, the PSSD signals associated with no TOF signal are considered to originate from the subsequent α decays of the implanted ERs. Figure 2 shows PSSD energy spectra in anticoincidence with the TOF in the ^{64}Ni$+^{154}$Sm reaction at all incident energies. The dashed lines indicate α-decay energies of known isotopes. It can be seen that the relative strengths of the α-decay peaks drastically change according to the reaction energy. At low energies, e.g., $E_{\mathrm{c.m.}}=175$ MeV, three peaks can be observed, which are considered to originate from the α-decay chain of ^{216}Th-^{212}Ra-^{208}Rn. These peaks disappear as the reaction energy increases, while other decay-chain peaks appear and then disappear. The strong α peaks were also used for the energy calibration of the PSSD (73 mm$\times$55 mm, 15 strips in the front face and 128 strips in the back face), as well as the 5.486-MeV α peak from an ^{241}Am source (shown in Fig. 2 at $E_{\mathrm{c.m.}}=190$ MeV). The typical energy resolution of the individual front strips was 70 keV (FWHM, full width at half maximum) and the horizontal and vertical position resolutions were 0.25 mm and 0.5 mm (FWHM), respectively.

The isotopes were identified by time- and position-correlation analysis of the α-decay events of ER-α_1-α_2 type, that is, the implanted ER and the subsequent α decays occurred within the time interval related to their half-lives at the same position within the PSSD resolution. Figure 3 shows a typical example in the ^{64}Ni+^{154}Sm reaction at $E_{\mathrm{c.m.}}=183$ MeV; (a) is the single energy spectrum of the α-decay particles and (b) is the two-dimensional spectrum of the energy E_α versus the time difference between the position-correlated ER and the subsequent α-decay particle, and (c) is the two-dimensional energy matrix of the correlated α_1-α_2 chains between the parent and the daughter nuclear decays. The maximum search times were 1000 sec for ER-α_1 in Fig. 3(b), 100 sec (closed symbols) and 10 000 sec (open symbols) for α_1-α_2 in Fig. 3(c). The boxes in the figure are guides to the eye for the various α-decay properties (α-decay energy E_α and lifetime τ) having an appropriate energy width of $E_\alpha \pm 50$ keV and $\frac{1}{10}\tau \leqslant \Delta T \leqslant 10\tau$. The dashed boxes are for the correlated α_1-α_3. Since the decay properties for some pairs of isotopes (e.g., ^{211}Ra and ^{212}Ra) are very similar to each other, definite identification between them was not achieved.

The ER cross sections for each evaporation channels were obtained by counting the ER-α_1 events thus identified. The number of ER-α_1 events, for example, 68 for ^{216}Th in Fig. 3(b) is consistent with the observed 37 α_1-α_2 chains for ^{216}Th-^{212}Ra in Fig. 3(c), because half of the α-decay events escape from the PSSD without depositing their full energy. For other cases, consistency was also obtained; for example, 234 events for ^{211,212}Ra are consistent with 19 chains for ^{211,212}Ra-^{207,208}Rn because the daughter nuclei ^{207}Rn and ^{208}Rn have an α-decay branching ratio less than 20% and 60%, respectively. The isotopes ^{211,212}Ra are considered to be not only the ER directly produced by $\alpha 3n$ and $\alpha 2n$ channels but also the decay product of ^{215,216}Th produced by $3n$ and $2n$ channels. For such αxn channels, the cross sections were obtained by subtracting the count of xn channels corresponding to their parent nuclei.

In order to obtain absolute values of the ER cross sections, the efficiency of the present detection system needs to be known. For this purpose, we previously measured the solid angle and the transmission efficiency of the RMS by using α particles from a source, elastic recoils, and evaporation residues produced in several reactions [13]. The measured efficiency was compared with an ion-optical calcula-

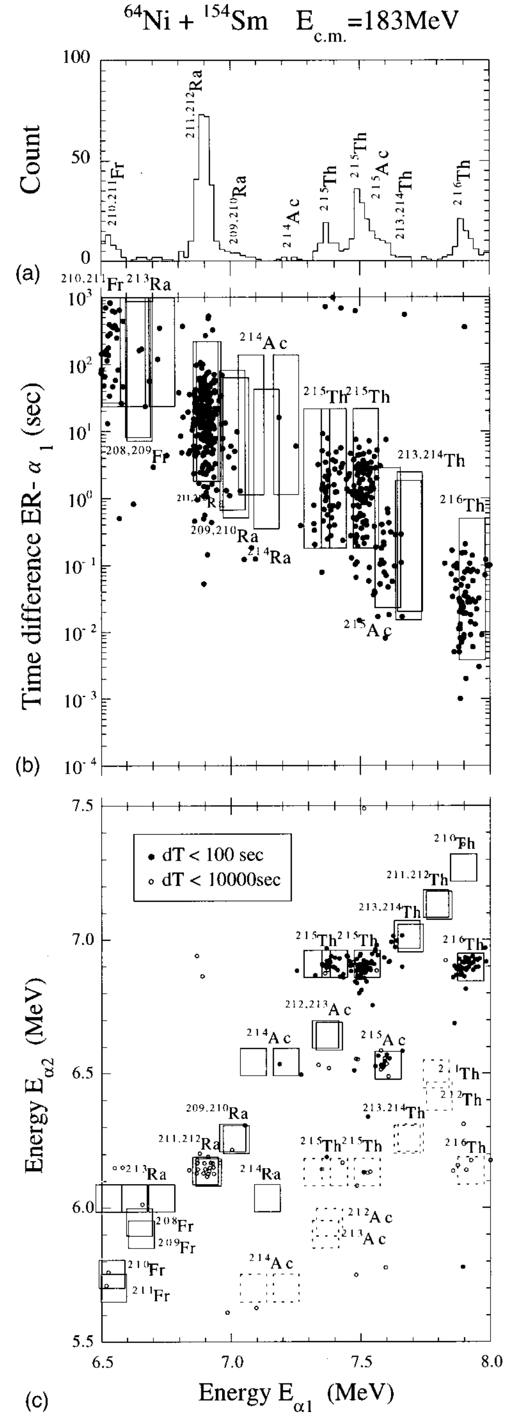

FIG. 3. Measured spectra as a function of the energy $E_{\alpha 1}$ in the ^{64}Ni+^{154}Sm reaction at $E_{\mathrm{c.m.}}=183$ MeV ($E_{beam}=269$ MeV). (a) Singles energy spectrum of the α-decay particles. (b) Two-dimensional matrix of E_α versus the time difference between the position-correlated ER and the subsequent α-decay particle. (c) Two-dimensional energy matrix of the correlated α_1-α_2 chains of the parent and the daughter nuclear decays. The maximum search times are (b) 1000 sec, (c) 100 sec (closed symbols), and 10 000 sec (open symbols). The boxes indicate the energy-time regions for the various α-decay properties of decay energy E_α and lifetime τ ($E_\alpha \pm 50$ keV and $\frac{1}{10}\tau \leqslant \Delta T \leqslant 10\tau$). The dashed boxes are for the correlated α_1-α_3.

tion of the code GIOS [14], and good agreement between them was obtained. In the present RMS setting of zero mass/charge dispersion, two charge states of ER were transported to the focal plane. The charge state distributions of low energy heavy recoils have also been measured and confirmed to be reproduced by the empirical Shima formula [15]. Energy and angular distributions were estimated by the statistical model code PACE2 [16], and the effects of energy loss and multiple scattering were estimated by the code TRIM [17]. The total efficiency of the present system was typically 18% and 10% for xn and αxn channels, respectively.

The ER cross sections thus obtained for xn, pxn, and αxn channels in the ^{64}Ni+^{154}Sm reaction are shown in Fig. 4 as a function of $E_{\mathrm{c.m.}}$ as well as excitation energy E_{ex}. Error bars include the statistical error in addition to a systematic error of 40% for the estimates of RMS transmission and ER distributions. The inverted triangles indicate the upper limit of the measurement, which were determined as a one-event counting yield when no ER was observed. The solid and dashed curves are the calculated results described in the following section.

III. THEORETICAL ANALYSIS AND DISCUSSION

In order to discuss the possible fusion enhancement or hindrance depending on the target deformation in tip and side collisions, we compared the measured excitation functions of ER cross sections with simple model calculations: first, the total fusion cross section in the entrance channel was estimated by a coupled channel calculation using the code CCDEF [18] and second, the survival probability of each ER in the exit channel was calculated using the statistical model code HIVAP [19]. Because the theoretical analysis is basically the same as the previous analysis for ^{60}Ni+^{154}Sm and ^{76}Ge+^{150}Nd [9,10], only the key points are mentioned here.

In the sub-barrier energy region, a large fusion enhancement has been observed due to the deformation of ^{154}Sm. Gomes *et al.* [20] measured fusion cross sections with the projectiles ^{4}He, ^{12}C, ^{16}O, ^{32}S, and ^{40}Ar and found that the static deformation of the ^{154}Sm target was the main cause responsible for the fusion enhancement. However, the best fit to the fusion cross sections was achieved when considering, in addition to the deformation, the coupling to the first 3^- state of the ^{154}Sm and the first 2^+ state of the projectile. The importance of static deformation on the sub-barrier fusion enhancement was also demonstrated by Lemmon *et al.* [21], in that the barrier distribution was well reproduced by the coupled channel calculations including quadrupole and hexadecapole deformations of the ^{154}Sm. In the present analysis for ^{64}Ni+^{154}Sm, fusion cross sections were calculated by using a simple coupled channel calculation CCDEF, to take account of the static target deformations together with the coupling of the inelastic channels to the fusion process. The parameters of the static quadrupole and hexadecapole deformations for the ^{154}Sm target are $\beta_2=0.321$ and $\beta_4=0.08$ [22], respectively. The couplings to the inelastic excitations of the low-lying vibrational states 2^+ ($\beta_2=0.207$) [23] and 3^- ($\beta_3=0.208$) [24] for the projectile ^{64}Ni and 3^- ($\beta_3=0.084$) [24] for the target ^{154}Sm were taken into account. The effect of an additional coupling to higher vibrational states of 2^+ (1.178 MeV) and 2^+ (1.44 MeV) of ^{154}Sm was very weak.

As for the statistical model calculation using HIVAP, the parameters used for ^{60}Ni+^{154}Sm have been confirmed in the same compound system of ^{32}S+^{182}W, where good agreement between the data and the calculated results for both the fusion-fission cross sections and the ER cross sections were obtained without any extra-extra-push energy [9]. For ^{64}Ni+^{154}Sm, the parameters were confirmed to reproduce the reported ER cross sections in the same compound system of ^{40}Ar+^{178}Hf [25]. In the region of thorium isotopes near the $N=126$ shell closure, the standard statistical model calculation generally overestimates the measured xn cross sections. This problem was solved by Junghans and co-workers [26,27] by taking into account collective enhancements of the level density for a deformed nucleus,

$$\rho(E)=K_{rot}K_{vib}\rho_{int}(E), \tag{1}$$

where K_{rot} and K_{vib} are the coefficients for rotational and vibrational enhancements, respectively, of the intrinsic level density $\rho_{int}(E)$ at excitation energy E. The value of K_{rot} (or K_{vib}) was set to 1.0 when the quadrupole deformation parameter β_2 is less (or larger) than 0.17 [26]. The β_2 values of the ground-state quadrupole deformation and the saddle-point deformation were taken from Refs. [12] and [28], respectively. Here, the level density parameter was assumed to be

$$a=\tilde{a}\{1+[1-\exp(-E/E_{sd})]\delta W/E\}. \tag{2}$$

A shell damping factor of $E_{sd}=18$ MeV was used [29], and the shell correction energy δW was the difference of the experimental mass [30] and the calculated liquid drop mass [31]. The asymptotic value of $\tilde{a}$ was given in Refs. [32,33]. The fission barrier height was given by $B_f=\alpha B_{LD}-\delta W$, where the liquid drop fission barrier B_{LD} was calculated according to Ref. [28]. The adjusting parameter α was set to 1.03.

The solid curves in Fig. 4 show the ER excitation functions thus calculated. Except for the absolute values of the cross sections, the calculated results reasonably reproduce the gross structure of the bell-shaped distribution such as the peak position and the width for each ER channel. For thorium isotopes, for example, ^{216}Th ($2n$ channel) has a peak at low excitation energy E_{ex} of about 25 MeV, and the peak energy shifts toward higher E_{ex} for ^{215}Th ($3n$), ^{214,213}Th ($4n$,$5n$) and ^{212,211}Th ($6n$,$7n$) according to their neutron separation energies of about 8–9 MeV. The same trend is shown for actinium isotopes ($p2n$–$p6n$), while the radium isotopes have two peaks corresponding to αxn and $2pyn$ channels ($x=0$–5 and $y=x+2$).

As for the absolute cross section, however, the calculated results largely overestimate the data especially in the low excitation channels like $2n$, $3n$, and $p2n$. This discrepancy gradually decreases as the number of evaporation particles increases, and finally good agreement is obtained for five to

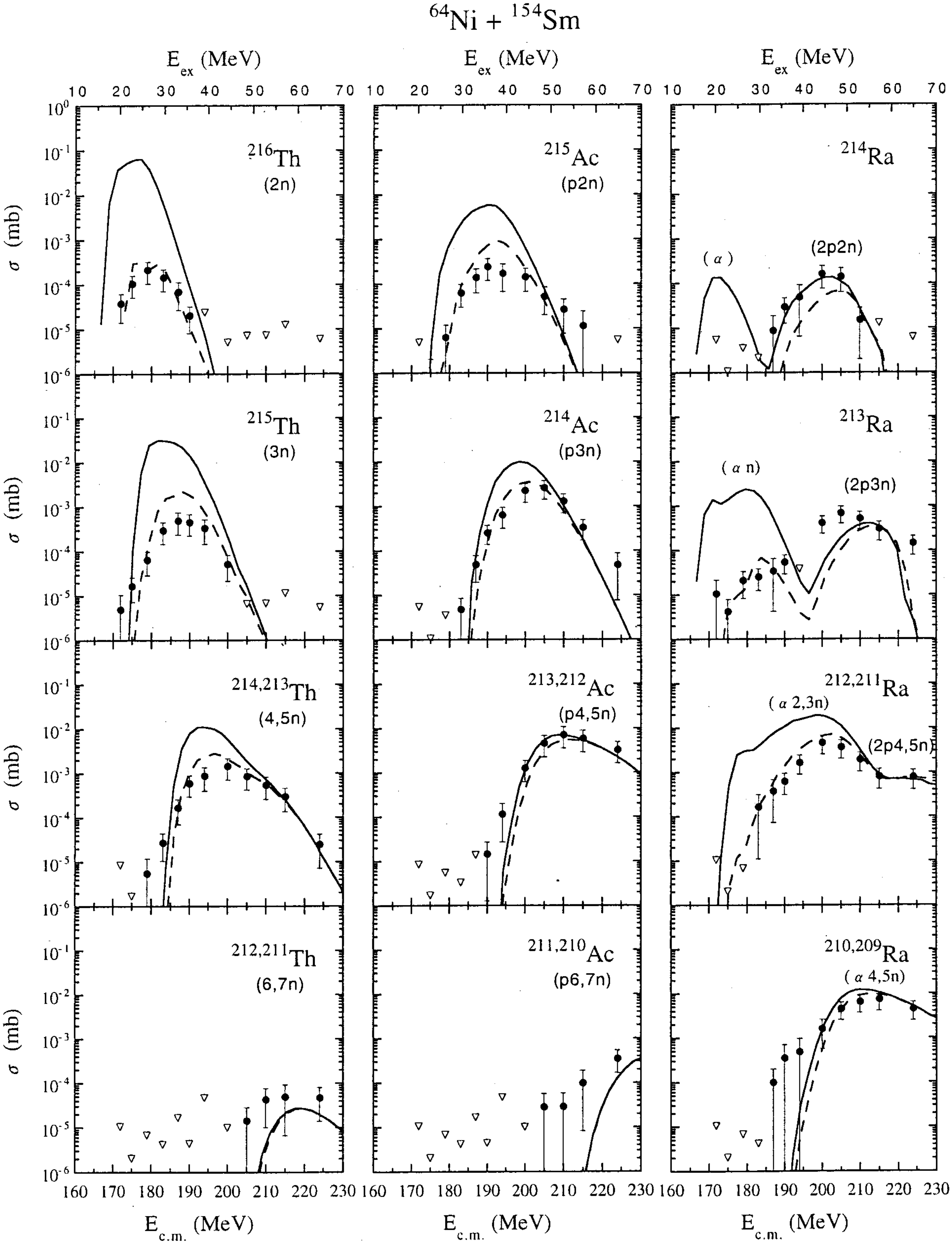

FIG. 4. Measured evaporation residue cross sections for xn, pxn, and αxn channels in the ^{64}Ni+^{154}Sm reaction as a function of $E_{c.m.}$ and excitation energy E_{ex}. The inverted triangles indicate the upper limit of the measurement, which were determined as a one-event counting yield when no ER was observed. The solid and dashed curves show the calculated results of HIVAP.

seven particle evaporation channels like $6n$, $7n$, $p4n$, $p5n$, $p6n$, $\alpha 4n$, and $\alpha 5n$. It is noted that no ER leading to ^{214}Ra was observed below $E_{\mathrm{c.m.}}=184$ MeV, in contrast with calculations for the α channel, whereas the $2p2n$ channel was well reproduced in the high $E_{\mathrm{c.m.}}$ region. The ERs of ^{213}Ra and ^{212,211}Ra also showed smaller yields than the calculated αn and $\alpha 2n, \alpha 3n$ channels, but for each of them, better agreement was observed for $E_{\mathrm{c.m.}} \gtrsim 190$ MeV. For the high excitation channels of $\alpha 4n, \alpha 5n$, the absolute cross sections of ^{210,209}Ra were well reproduced.

A similar situation has also been observed in the ^{60}Ni $+{}^{154}$Sm reaction system as reported in our previous paper [9]; i.e., good agreement between the data and the calculated results was obtained in the high energy region of $E_{\mathrm{c.m.}} \gtrsim 200$ MeV, while a large hindrance of the ER cross sections occurred below the Bass barrier. At the lowest energies of $E_{\mathrm{c.m.}}=175$ and 182 MeV, there was no event observed corresponding to ^{212,211}Th $(2n,3n)$, ^{211,210}Ac $(p2n,p3n)$, ^{210,209}Ra $(\alpha,\alpha n)$, and ^{209,208}Ra $(\alpha,\alpha pn)$. Because the previous measurements at these energies gave only an upper limit, the ER cross sections were measured again in the present experiment with about ten times better statistics at $E_{\mathrm{c.m.}}=182$ MeV (and also 207 MeV for reconfirmation). The measured ER cross sections of 2.5 ± 1.3 nb and 5.5 ± 2.5 nb for $2n,3n$ and $\alpha,\alpha n$ channels, respectively, were considerably smaller than the predictions. The hindrance factor of the measured cross sections in these low energy regions was typically about 10^3.

These facts mentioned above become quite obvious when extracting the xn channels as shown in Fig. 5. The thick solid curve with error bars and the dashed curve are the sum of measured and calculated xn cross sections, respectively. Reasonably good agreement between them is shown in the high energy region $E_{\mathrm{c.m.}} \gtrsim 200$ MeV. The calculated results, however, gradually deviate from the observed cross sections as the reaction energy $E_{\mathrm{c.m.}}$ is decreased. The maximum discrepancy amounts to about three orders of magnitude at the lowest energy $E_{\mathrm{c.m.}}=172$ MeV. The calculated results of the CCDEF are also shown in Fig. 5. The solid (dotted) line is the calculated result with (without) both effects of static target deformation and inelastic couplings, and the dashed line is with target deformation alone. The importance of target deformation on the sub-barrier fusion enhancement is clearly shown, because the $2n,3n$ channel has a certain cross section below the Bass barrier energies indicated by the dotted line, although large fusion hindrance occurred.

The inset in Fig. 5 shows the fusion barrier V depending on the colliding angle θ of the ^{64}Ni projectile with respect to the orientation of the symmetric axis of the deformed ^{154}Sm target. The barrier height becomes minimized around $E_{\mathrm{c.m.}} \sim 170$ MeV for near tip collisions ($\theta=0°-10°$) and maximized around $E_{\mathrm{c.m.}} \sim 200$ MeV in side collisions ($\theta=60°-90°$). Although collisions for all possible orientations occur at above-barrier energies $E_{\mathrm{c.m.}} \gtrsim 200$ MeV, it is considered that near side collisions mainly contribute because of their large solid angle compared to that of the tip collisions. From the fact that small fusion hindrance is observed in the higher energy region and large hindrance in the lower energy region, it is considered that near side collisions lead the system to complete fusion and near tip collisions do not always form a compound nucleus. In other words, the actual fusion barrier at the tip collision is larger than the calculated barrier.

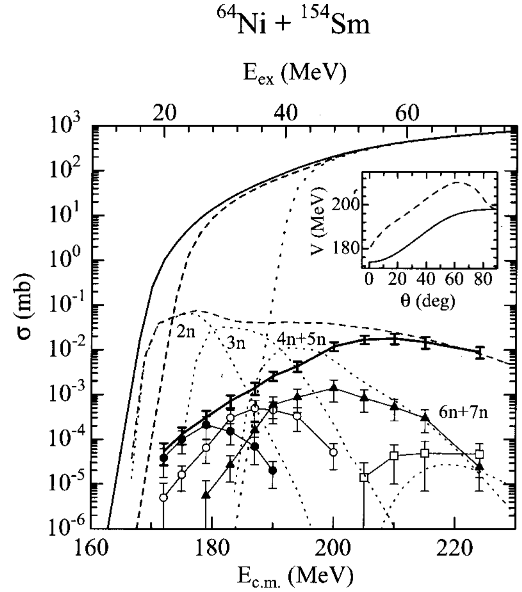

FIG. 5. Measured excitation functions in the ^{64}Ni$+{}^{154}$Sm reaction for xn channels ($2n$, solid circles; $3n$, open circles; $4n+5n$, solid triangles; $6n+7n$, open squares). The thick solid curve with error bars and the dashed curve are the sum of the measured and the calculated xn cross sections, respectively. The slopes from around 10^3 mb are the calculated results of the CCDEF; the solid (dotted) slope is with (without) both the effects of static target deformation and inelastic couplings, and the dashed slope is with target deformation alone. The inset is the fusion barrier V depending on the colliding angle θ of ^{64}Ni projectile with respect to the orientation of the symmetric axis of the deformed ^{154}Sm target. The solid curve in the inset is the original barrier and the dashed curve is the modified barrier (see text).

In order to confirm this consideration, we recalculated the ER cross sections by adding a certain extra-extra-push energy E_{xx} to the original barrier V depending on the colliding angle θ. This means that larger E_{xx} is needed for tip collisions than for side collisions, as indicted by the dashed curve in the inset of Fig. 5. The calculated results for all measured ER cross sections are shown by the dashed curves in Fig. 4. The dashed curves well reproduce the experimental ER cross sections even in the sub-barrier region, better than the solid curves with the original barrier height. This supports our simple assumption, i.e., a larger E_{xx} is needed for tip collisions than for near side collisions. The same conclusion was reached for the fusion reactions of ^{60}Ni$+{}^{154}$Sm [9] and ^{76}Ge$+{}^{150}$Nd [10]. The present result is also consistent with the conclusion obtained by Hinde *et al.* in the ^{16}O$+{}^{238}$U reaction [34]; side collisions with the deformed nucleus ^{238}U lead to fusion-fission while tip collisions undergo quasifission without forming a fully equilibrated compound nucleus. The present result shows that side collisions have the advantage of small fusion hindrance, consistent with the prediction

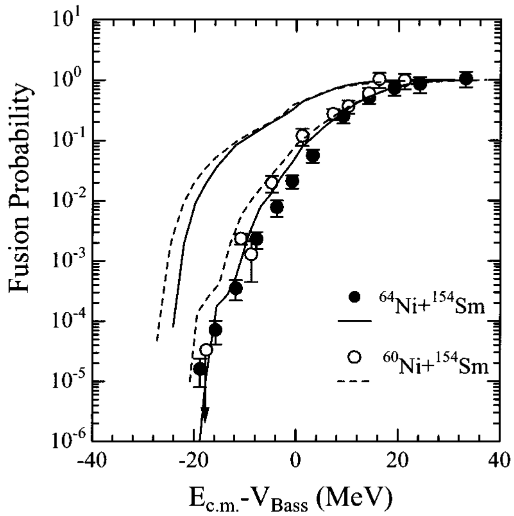

FIG. 6. Fusion probability for the reactions $^{64}Ni+^{154}Sm$ (solid circles and solid curves) and $^{60}Ni+^{154}Sm$ (open circles and dashed curves), extracted by summing total measured evaporation residue cross sections with the aid of the calculated survival probabilities from HIVAP. The curves are the calculated results of CCDEF with the original and modified fusion barrier (see text).

of hugging fusion. This is the entrance channel effect obtained by using deformed nuclei as the reaction partners. However, at the same time, side collisions have the disadvantage of a small survival probability in the exit channel because of high excitation energy.

In general, the ER survival probability against fission is very sensitive not only to the excitation energy but also to the separation energies of emitted light particles relative to the fission barrier. The ratio Γ_n/Γ_f of neutron emission width to fission width is roughly proportional to $\exp[(B_f - B_n)/T]$, where T is the nuclear temperature of the compound nucleus. In the thorium isotope region, the fission barrier B_f has a peak at the $N=126$ shell closure, and the neutron binding energy B_n gradually decreases as the mass number increases, although there is an odd-even effect. For the even-even isotope ^{214}Th, which is the compound nucleus formed in $^{60}Ni+^{154}Sm$, B_n is larger by about 1 MeV than B_f, while ^{218}Th formed in $^{64}Ni+^{154}Sm$ has a smaller B_n than B_f. This small neutron separation energy would produce a larger survival probability. In fact, the experimental cross sections for each ER channel in the ^{64}Ni-induced reaction were about 10–100 times larger than that in the ^{60}Ni-induced reaction. It is of interest to see whether such enhancement comes only from the exit channel or also from the entrance channel in the case of the more *n*-rich projectile ^{64}Ni. To see the entrance channel effect, the fusion probability was extracted from the measured total ER cross sections with the aid of the calculated survival probability in the same manner as our previous analysis described in Ref. [11] in detail. As shown in Fig. 6, no obvious difference between the ^{64}Ni- and ^{60}Ni-induced reactions was observed in the excitation functions normalized by the Bass barrier. In both reaction systems, the fusion probabilities in the low energy region corresponding to tip collisions were significantly smaller than the simple coupled channel calculations by three orders of magnitude, whereas no hindrance was observed above $E_{c.m.} - V_{Bass} \sim 20$ MeV. Although there was no evident effect of the *n*-rich projectile on complete fusion, the orientation effect of the target deformation was clearly observed in the entrance channel.

It is worth considering the entrance channel effect due to the deformation by comparing with the contact point of the colliding nuclei and the fission saddle point of the compound nucleus. A tip collision gives the maximum value of the distance R/R_0 between the mass centers of the colliding nuclei at the contact point, where R_0 is the radius of the compound nucleus. In the present system of $^{64}Ni+^{154}Sm$, the position of the maximum distance $R_{max}/R_0 = 1.77$ at the tip collision is well outside the saddle point $R_{saddle}/R_0 \sim 1.5$ [35] of the compound nucleus ^{218}Th. Consequently, a tip collision would need extra energy to surmount the saddle point on the potential surface towards compound nucleus formation. A side collision, on the other hand, would minimize the kinetic energy loss in the fusion process because the ratio $R_{min}/R_0 = 1.48$ implies that the contact point is closer to the position of the saddle point. This supports the original speculation that the compact touching configuration of side collisions is more favorable for fusion than the elongated configuration. Here, in the cases of the previous $^{32}S+^{182}W$ system and ^{154}Sm target systems with projectiles lighter than ^{40}Ar, complete fusion can occur irrespective of the deformed target orientations, because even the maximum distance achieved during a tip collision is well inside the saddle point of the compound nucleus.

IV. SUMMARY

We have measured the excitation functions of the ER cross sections for xn, pxn, and αxn channels in the $^{64}Ni + ^{154}Sm$ reaction at energies around the Coulomb barrier. The orientation effect of the deformed nucleus was clearly observed when the measured cross sections were compared with the coupled channel calculation CCDEF for the fusion process (entrance channel) and the statistical model calculation HIVAP for the evaporation process (exit channel). Complete fusion certainly occurred for small collision angles in the energy region below the Bass barrier, but was largely hindered by almost three orders of magnitude, while a small fusion hindrance was observed in the higher energy region. This sub-barrier fusion hindrance was investigated by taking into account the orientation angle of the ^{64}Ni projectile with respect to the deformed ^{154}Sm target at the contact point. By assuming that a larger extra kinetic energy was needed for near tip collisions than for side collisions, the measured excitation functions of the ER channels were well reproduced.

The present result is consistent with our previous conclusion for the fusion reactions of heavy projectiles ^{60}Ni and ^{76}Ge with well-deformed targets ^{154}Sm and ^{150}Nd, respectively [9,10]. It was found that near tip collisions needed some extra kinetic energy to surmount the saddle point, because the distance between the mass centers of the colliding nuclei is larger than the saddle position of the compound nucleus, while near side collisions would favor fusion occurring inside the saddle. This supports the original speculation of gentle fusion and hugging fusion that the compact touching configuration of the side collision is more favorable for complete fusion than the elongated configuration. By comparing the data between the ^{64}Ni-induced and ^{60}Ni-induced reactions, it was found that the ER cross sections in the former reaction were about 100 times larger than those in the latter reaction. This is an exit channel effect due to the large survival probability of a more *n*-rich compound system. The fusion probability for both reaction systems was obtained from the measured ER cross sections by using the calculated survival probability. There was no obvious difference between two isotopes differing by four neutrons, thus failing to show the expected entrance channel effect for more *n*-rich projectile systems. This is also consistent with the recent results using *n*-rich radioactive beams in the reactions of ^{27,29,31}Al+^{197}Au [36] and ^{32,38}S+^{181}Ta [37].

[1] S. Hofmann *et al.*, Z. Phys. A **350**, 277 (1995); **350**, 281 (1995); **354**, 229 (1996).
[2] Y.A. Lazarev *et al.*, Phys. Rev. Lett. **73**, 624 (1994); **75**, 1903 (1995); Phys. Rev. C **54**, 620 (1996).
[3] S. Hofmann and G. Münzenberg, Rev. Mod. Phys. **72**, 733 (2000).
[4] W.D. Myers and W.J. Swiatecki, Phys. Rev. C **62**, 044610 (2000).
[5] V.Yu. Denisov, Prog. Part. Nucl. Phys. **46**, 303 (2001).
[6] W. Nörenberg, *Proceedings of the International Workshop on Heavy-Ion Fusion*, Padova, Italy (World Scientific, Singapore, 1994), p. 248
[7] A. Iwamoto, P. Möller, J.R. Nix, and H. Sagawa, Nucl. Phys. **A596**, 329 (1996).
[8] H. Ikezoe, Y. Nagame, T. Ikuta, S. Hamada, I. Nishinaka, and T. Ohtsuki, Nucl. Instrum. Methods Phys. Res. A **376**, 420 (1996).
[9] S. Mitsuoka, H. Ikezoe, K. Nishio, and J. Lu, Phys. Rev. C **62**, 054603 (2000).
[10] K. Nishio, H. Ikezoe, S. Mitsuoka, and J. Lu, Phys. Rev. C **62**, 014602 (2000).
[11] K. Nishio, H. Ikezoe, S. Mitsuoka, K. Satou, and S.C. Jeong, Phys. Rev. C **63**, 044610 (2000).
[12] P. Möller, J.R. Nix, P. Armbruster, S. Hofmann, and G. Münzenberg, Z. Phys. A **359**, 251 (1997).
[13] T. Kuzumaki, H. Ikezoe, S. Mitsuoka, T. Ikuta, S. Hamada, Y. Nagame, I. Nishinaka, and O. Hashimoto, Nucl. Instrum. Methods Phys. Res. A **437**, 107 (1999).
[14] H. Wollnik, J. Brezima, and M. Berz, Nucl. Instrum. Methods Phys. Res. A **258**, 408 (1987).
[15] K. Shima, T. Ishihara, and T. Mikumo, Nucl. Instrum. Methods Phys. Res. **200**, 605 (1982); K. Shima, N. Kuno, and M. Yamanouchi, Phys. Rev. A **40**, 3557 (1989).
[16] A. Gavron, Phys. Rev. C **21**, 230 (1980).
[17] J.F. Ziegler, J.P. Biersack, and U. Littmark, *The Stopping and Range of Ions in Solids* (Pergamon, New York, 1985).
[18] J. Fernandez-Niello, C.H. Dasso, and S. Landowne, Comput. Phys. Commun. **54**, 409 (1989).
[19] W. Reisdorf and M. Schädel, Z. Phys. A **343**, 47 (1992).
[20] P.R.S. Gomes, I.C. Charret, R. Wanis, G.M. Sigaud, V.R. Vanin, R. Liguori Neto, D. Abriola, O.A. Capurro, D.E. DiGregorio, M. diTada, G. Duchene, M. Elgue, A. Etchegoyen, J.O. Fernandez Niello, A.M.J. Ferrero, S. Gil, A.O. Macchiavelli, A.J. Pacheco, and J.E. Testoni, Phys. Rev. C **49**, 245 (1994).
[21] R.C. Lemmon, J.R. Leigh, J.X. Wei, C.R. Morton, D.J. Hinde, J.O. Newton, M. Dasgupta, and N. Rowley, Phys. Lett. B **316**, 32 (1993).
[22] P. Raghavan, At. Data Nucl. Data Tables **42**, 189 (1989).
[23] S. Raman, C.H. Malarkey, W.T. Milner, C.W. Nestro, Jr., and P.H. Stelson, At. Data Nucl. Data Tables **36**, 1 (1987).
[24] R.H. Spear, At. Data Nucl. Data Tables **42**, 55 (1989).
[25] D. Vermeulen, H.G. Clerc, C.C. Sahm, K.H. Schmidt, J.G. Keller, G. Munzenberg, and W. Reisdorf, Z. Phys. A **318**, 157 (1984).
[26] A.R. Junghans, M. de Jong, H.G. Clerc, A.V. Ignatyuk, G.A. Kudyaev, and K.H. Schimidt, Nucl. Phys. **A629**, 635 (1998).
[27] A.S. Iljinov, M.V. Mebel, N. Bianchi, E. de Sanctis, C. Guaraldo, V. Luchierini, V. Muccifora, E. Polli, A.R. Reolon, and P. Rossi, Nucl. Phys. **A543**, 517 (1992).
[28] S. Cohen, F. Plasil, and W.J. Swiatecki, Ann. Phys. (N.Y.) **82**, 557 (1974).
[29] A.V. Ignatyuk, G.N. Smirenkin, and A.S. Tishin, Sov. J. Nucl. Phys. **21**, 255 (1975).
[30] G. Audi and A.H. Wapstra, Nucl. Phys. **A595**, 409 (1995).
[31] W.D. Myers and W.J. Swiatecki, Ark. Fys. **36**, 343 (1967).
[32] W. Reisdorf, Z. Phys. A **300**, 227 (1981).
[33] W.D. Myers and W.J. Swiatecki, Ann. Phys. (N.Y) **84**, 186 (1974).
[34] D.J. Hinde, M. Dasgupta, J.R. Leigh, J.C. Mein, C.R. Morton, J.O. Newton, and H. Timmers, Phys. Rev. C **53**, 1290 (1996).
[35] P. Möller, J.R. Nix, W.D. Myers, and W.J. Swiatecki, At. Data Nucl. Data Tables **59**, 185 (1995).
[36] Y.X. Watanabe, A. Yoshida, T. Fukuda, T. Sekine, Y. Watanabe, H. Ikezoe, Y. Nagame, T. Ikuta, I. Nishinaka, Y. Mizoi, J. Nakano, M. Hirai, H. Sakurai, H. Kobinata, Y. Pu, K. Kimura, and M. Ishihara, Eur. Phys. J. A **10**, 373 (2001).
[37] K.E. Zyromski, W. Loveland, G.A. Souliotis, D.J. Morrissey, C.F. Powell, O. Batenkov, K. Aleklett, R. Yanez, and I. Forsberg, Phys. Rev. C **63**, 024615 (2001).